J. Fluid Mech. (2025), *vol.* 1019, A39, doi:10.1017/jfm.2025.10624

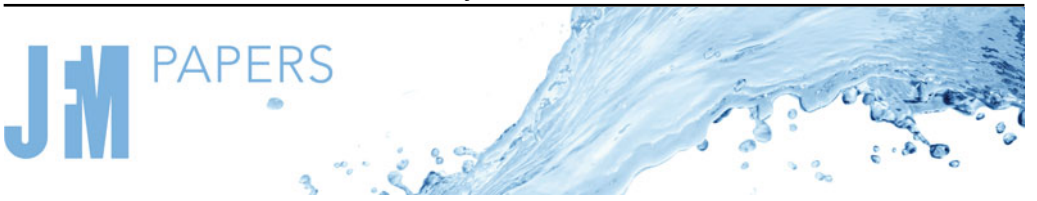

Theory of soft active equilibrium wetting

Ghansham Rajendrasingh Chandel[1] **and Siddhartha Das**[1]

[1]Department of Mechanical Engineering, University of Maryland at College Park, MD, USA

Corresponding author: Siddhartha Das, sidd@umd.edu

(Received 13 December 2024; revised 16 July 2025; accepted 22 August 2025)

We must address active matter in the context of soft boundaries to bridge the gap between our understanding of active matter and the dynamics of biological systems (represented as active matter) under natural conditions. However, the physics of such active drops (matter) in contact with a soft and deformable surface has remained elusive. In this paper, we attempt to fill this gap and develop a theory for soft, active wetting. Our theory, which accounts for the various free energies for passive substrate and active drops as well as the active stresses, provides an equilibrium description of (active) particle orientation inside the drop and an equilibrium shape of the drop–soft-solid system. We obtain an analytical equation relating the activity to the internal pressure of an active drop. The equilibrium calculation further yields an ordered state of the polarisation field inside the drop. As compared to the non-active drops, the active drops with extensile activity press more into the soft surface, while the active drops with contractile activity either rise out of the soft surface (for smaller magnitude of negative activity) or make the soft surface bulge (for larger magnitude of negative activity). Finally, the three-phase contact line undergoes a rotation that depends on the strength of activity. These findings shed light on the manner in which the active stresses interact with surface tension and elasticity at the fundamental level.

Key words: active matter, drops, wetting and wicking

1. Introduction

Active matter (AM) is ubiquitous in life sciences; from collective cell migration in cancer and growing or healing tissues (Balasubramaniam, Mège & Ladoux 2022; Trepat *et al.* 2009; Drescher *et al.* 2011), to bacterial colonies (Peng *et al.* 2016; Sengupta 2020), to microtubules transport (Kim *et al.* 2018; Tan *et al.* 2019). It is commonplace to encounter AM over soft backgrounds in both *in vitro* and *ex vivo* processes. Soft substrates (SS), which can be the elastic cell walls, tissues, vesicles or majorly fluid substrate (like mucus), have elasticity ranging from 0 to 10^3 Pa (Levental, Georges & Janmey 2007,

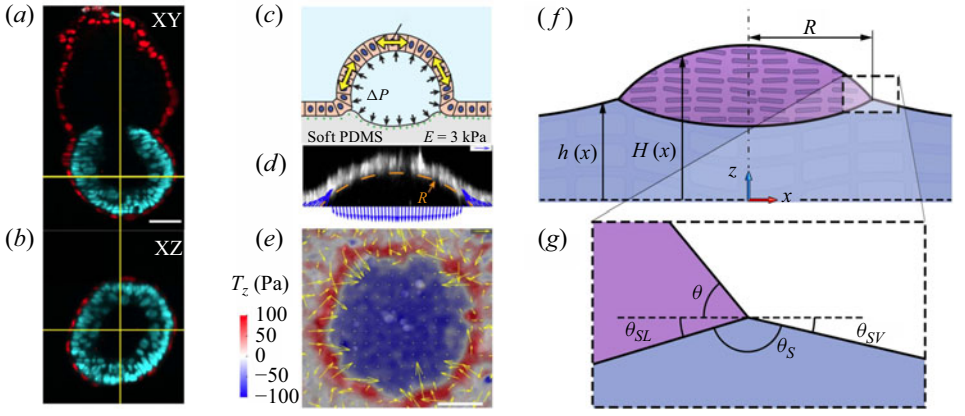

Figure 1. (*a*,*b*) Immunofluorescence image of *in utero* implanted fertilised mouse embryo from side and top, respectively. Blue regions are epiblast cells that eventually form the embryo's body; red region is extra-cellular matrix. Panels (*a*) and (*b*) have been reproduced from Ichikawa *et al.* (2022). (*c*) Study of drops enclosed by epithelial cells on soft substrates. (*d*) Side view and (*e*) Top view with corresponding stress distribution inside the drop. Panels (*c*)–(*e*) have been reproduced from Latorre *et al.* (2018). (*f*) Schematic of the active drop on soft substrate with different angles identified in panel (*g*).

Soofi *et al.* 2009, Singh & Chanda 2021); at lengths scales associated with active matter (1–100 μm), surface tension (ST) becomes a dominating force in such systems. Therefore, the hydrodynamics of active matter is invariably coupled to the substrate shape, which, in turn, is coupled to the active ordering due to the active stresses. For example, Guruciaga *et al.* (2024) used Landau's theory to describe the geometry of the first cells of fertilised mouse embryo on soft background (e.g. Matrigel and uterine wall Ichikawa *et al.* 2022) (see figure 1*a*,*b*) that were simplistically modelled as a spherical cap of fixed radius. Typically, the active stresses produced from directional cellular activity consistently range from 0.1 to 1 kPa (Saw *et al.* 2017; Bazellières *et al.* 2015; Trepat *et al.* 2009); such stresses, coupled with the elasticity of the biological tissues that surround these cellular systems, will ensure that elasto-capillarity will determine the geometry and influence of the surrounding background. Furthermore, Latorre *et al.* (2018). demonstrated how active stresses imparted by the epithelial cells (which follow nematic ordering) dictate the overall shape of fluid filled bumps (figure 1*c*–*e*); however, in the theoretical description of the system, the directionality of the active stresses was disregarded (Pérez-González *et al.* 2019; Guillamat *et al.* 2022). While an *a priori* assumption on the deformed state of the substrate (Pérez-González *et al.* 2019; Guruciaga *et al.* 2024) can give us some insights into the developmental topology of that particular system, or an isotropic-state assumption can provide a solution for a simplified shape, the question of what topological deviations result from conditions of greater (or lesser) stiffness for varying active arrangements remains unaccounted for; in short, a rigorous theory of active matter (or active drops) on soft substrates remains missing in the existing literature.

In this paper, we provide a theory of active matter or active drop on soft substrates: we denoted it as the theory of soft active equilibrium wetting (figure 1*f*,*g*). The theory accounts for various free energies and active stresses associated with the active-drop–soft-substrate interactions and provide an equilibrium picture of the orientation of active particles inside the drop and the shape of the drop–substrate system. There are three key findings. First, we recover the equilibrium ordered state of the polarisation field as described by the Landau–de Gennes theory (Ramaswamy 2010; Ravnik & Žumer 2009). Second, through the development of a fundamental equation relating the drop shape to a

combination of activity and the drop internal pressure, we show that in comparison to a neutral drop, an active drop with extensile activity presses down more on the substrate, thereby increasing the wetting radius. This same equation is used to demonstrate that in comparison to the neutral drop, the active drop with contractile activity, however, can either raise above the substrate more (and consequently decrease the wetting radius) for a smaller magnitude of negative activity, or can make the substrate itself bulge (with an increased wetting radius) for a larger magnitude of negative activity. Last, we find that the three-phase contact line (TPCL) undergoes a rotation that depends on the strength of activity. Thus, our findings reveal the trifecta of mechanisms dictating the soft active wetting: substrate elasticity resisting shape change, capillary pressure pressing the substrate isotropically and the directional active stresses contributing predominantly to the drop curvature. These results challenge the intuition that the bulk active stress stretches or squeezes the substrate directly into a deformed shape; rather, at least for slender drops, active stresses effectively increase or decrease the contribution of the surface tension in elastocapillary deformation.

2. Mathematical description of the system

We start by considering a set-up where the mass of the active matter rests on a soft substrate. Such a set-up mirrors systems such as elongated cells on soft tissues, drops with microtubules over kinesin motors, lumen formation during embryonic development or muscle cells contracting soft tissues. In other words, the active drops that we consider are collections of active particles (or collections of active biological cells), as opposed to liquid drops containing suspended active particles. From the mathematical standpoint, our system consists of two parts: the first part ($\mathscr{F}_{tot}$) that can be expressed in a variational form (i.e. terms that can be represented as gradients of energy functional) and second, the non-variational terms that alter the equilibrium conditions through activity, pulling the system out of its lowest energy state.

2.1. *Expression for free energies of the system*

We can write

$$\mathscr{F}_{tot} = \int \mathrm{d}x\ f(h, H, \boldsymbol{p}) = \mathscr{F}_S + \mathscr{F}_{El} + \mathscr{F}_\gamma + \mathscr{F}_{spo} + \mathscr{F}_{el} + \mathscr{F}_{coupl} + F_1 + F_2, \quad (2.1)$$

where f is the free energy density. Following Jing, Sinha & Das (2017),

$$\mathscr{F}_S = \int_{-\infty}^{\infty} \mathrm{d}x\ \gamma_S \left(1 + h'^2\right)^{1/2}. \quad (2.2)$$

Here, $\mathscr{F}_S$ represents the surface energy of the substrate, and h and γ_S are the height and the surface tension of the substrate. For us, $\gamma_S(x) = \gamma_{SV}$, that is, the vapour–solid surface tension for $|x| > R$ and $\gamma_S(x) = \gamma_{SL}$, or vapour–liquid surface tension for $|x| \leqslant R$, where R is the radius of the active drop in consideration. Second,

$$\mathscr{F}_{El} = \int_{-\infty}^{\infty} \frac{\mathrm{d}q}{\sqrt{2\pi}\,\hat{K}(q)} \left[\hat{h}(q)\hat{h}(-q)\right] \quad (2.3)$$

is the elastic energy stored in the deformed solid; here, $\hat{h}(q)$ is the Fourier transform of the height and $\hat{K}(q) = (2E|q|/3)^{-1}$ is the kernel for a semi-infinite elastic solid in Fourier

space (Jerison *et al.* 2011; Lubbers *et al.* 2014). Moving forward, we have

$$\mathscr{F}_{\gamma} = \int_{-R}^{R} \mathrm{d}x\, \gamma \left(1 + H'^{2}\right)^{1/2}, \tag{2.4}$$

where $\mathscr{F}_{\gamma}$ is the surface energy of the liquid phase (active matter), γ is the liquid–vapour surface tension and H is the liquid–vapour interface height. It is worthwhile to discuss the meaning of H here. Unlike traditional drops, where the definition of the height of the drop is meaningful at scales sufficiently larger than atomic scale (usually above a few nanometres), with active drops, the validity of a definition of a sharp interface, such as a liquid–vapour interface, depends highly on the type of active matter under consideration. This is due to the fact that the continuum theories pertaining to active matter average the field variables (such as active stress, polarisation field, free-energy density, etc.) over several particles, as opposed to several molecules. In the context of soft boundaries, the active drops that we consider here are cellular colonies and our consequent theories must not make any predictions below sub-μm scale (or the scale much smaller than the size of a single cell) about the physical system. Put simplistically, the lower limit of the drop height H is set by the size of a single cell and, accordingly, this lower limit is much larger than the sub-μm scale. As a further note, we would like to point out here that there can be other types of active drops (different from those that we consider here), such as the suspension of swimming bacteria, chemical liquid crystals or drops with Janus particles. Such active drops, which are suspensions of active particles in liquids, are subject to similar interfacial phenomenon as regular drops.

Next, the terms $\mathscr{F}_{spo}$, $\mathscr{F}_{el}$ and $\mathscr{F}_{coup}$ represent the energies associated with the active particles (and, hence, the polarisation field $\boldsymbol{p}$) and are denoted as spontaneous energy, elastic energy and coupling energy, respectively (Trinschek *et al.* 2020). As discussed previously, the active drops considered in the paper are a collection of active cells and, thus, we do not see the Van der Waals interactions that happen near the solid–liquid and liquid–vapour interface. These particles are mostly directional in nature and the polarisation field ($\boldsymbol{p}$) reflects, approximately, the directionality of these particles (Ravnik & Žumer 2009). We express $\mathscr{F}_{spo}$ as

$$\mathscr{F}_{spo} = \int_{-R}^{R} \mathrm{d}x\, (H-h) \left[\frac{c_{sp4}}{4}(\boldsymbol{p}\cdot\boldsymbol{p})^2 - \frac{c_{sp2}}{2}\left(1 - 2\beta\kappa(H-h)\right)(\boldsymbol{p}\cdot\boldsymbol{p})\right]. \tag{2.5}$$

For active systems, $\mathscr{F}_{spo}$ ensures that at a film height smaller than the fluid adsorption layer thickness (H_a), which is typically a few molecules thick, the disordered state ($\boldsymbol{p} = \boldsymbol{0}$) is preferred, while with an increasing film thickness, in the absence of noise, all particles align in a spontaneous direction. In (2.5), c_{sp4} and c_{sp2} are parameters that determine how strongly the particles align in the ordered state and β is the adjusting parameter for height above which the particles start aligning in the ordered state. Finally, the variable κ appearing in (2.5) is as

$$\kappa(H-h) = \frac{H_a f_w(H-h)}{(H-h) f_w(H_a)}, \tag{2.6}$$

where f_w is the wetting energy that can expressed in terms of the Hamaker constant A as

$$f_w(u) = A\left(-\frac{1}{2u^2} + \frac{{H_a}^3}{5u^5}\right). \tag{2.7}$$

Here, κ ensures that below a certain height, the spontaneous arrangement of active particles is hindered due to geometric constraints. Consideration of this wetting energy (see (2.7)) is equivalent to considering a disjoining pressure Π, which can be related to $f_w(h)$ as $\Pi(h) = -(\partial f_w/\partial h) = -A((1/h^3) - (H_a^3/h^6))$. This expression of the disjoining pressure clearly reproduces the well-known disjoining pressure scaling, where $\Pi(h)$ varies as A/h^3 (where h is the local thickness). This expression obtained here includes an additional term $(A(H_a^3/h^6))$ which includes H_a. This additional term is a correction to a purely vdW-force-based disjoining pressure, as below a certain height (H_a), the molecular repulsion overtakes the vdW attraction. Please note that for the present case, in (2.6), $H >> H_a$, stemming from the fact that the lower limit of the drop height (H) is determined by the size of the cell that has a length scale of several microns. More importantly, it is because of this consideration that in our final calculations, we have not considered the effect of either the wetting energy or the disjoining pressure. In other words, we say that our theory is not to be taken to the length scales where the wetting energy or, equivalently, the disjoining pressure become important. Despite disregarding the effect of f_w and Π in our final calculations, we still retain their expressions in our paper for the sake of completeness, given the fact that the main paper (Trinschek *et al.* 2020) from which we obtain the different free energy expressions used in our calculation considered this expression for f_w as it probed the equilibrium of active liquid drops (or drops of liquids suspended with active particles). Therefore, if one aims to extend the theory to drops of liquids suspended with active particles or drops of chemical liquid crystals, they must account for the wetting energy into their energy functional to resolve the drop dynamics at TPCL. Further, we have

$$\mathscr{F}_{el} = \int_{-R}^{R} \mathrm{d}x\ (H-h)\frac{c_p}{2}\ (\boldsymbol{\nabla p} : \boldsymbol{\nabla p}) \tag{2.8}$$

as the elastic energy of the active matter (c_p is the corresponding elasticity). Finally, the contribution

$$\mathscr{F}_{coupl} = \int_{-R}^{R} \mathrm{d}x\ \left[\frac{c_{hp}}{2}\ (\boldsymbol{p}\cdot\boldsymbol{\nabla} h)^2 + \frac{c_{Hp}}{2}\ (\boldsymbol{p}\cdot\boldsymbol{\nabla} H)^2\right] \tag{2.9}$$

couples $\boldsymbol{p}$ to the drop surface and accounts for contributions where particles, depending on c_{Hp} and c_{hp}, either align themselves in parallel or terminate perpendicularly to the film surface at the drop–vapour and drop–solid boundaries, respectively. For our slender two-dimensional (2-D) system, we cannot reorient $\boldsymbol{p}$ in the depth direction (Trinschek *et al.* 2020) and, hence, $\mathscr{F}_{coupl}$ is constant for 2-D drops. Finally, in (2.1), F_1 and F_2 ensure two necessary system constraints. Here,

$$F_1 = \mathbb{P}\left[V - \int_{-R}^{R} \mathrm{d}x(H-h)\right] \tag{2.10}$$

ensures for volume conservation, while

$$\begin{aligned} F_2 = {} & \lambda_{SL}\left[H(R) - h(R^-)\right] + \lambda_{SV}\left[H(R) - h(R^+)\right] \\ & + \lambda_{SL}\left[H(-R) - h(-R^+)\right] + \lambda_{SV}\left[H(-R) - h(-R^-)\right] \end{aligned} \tag{2.11}$$

ensures drop–solid interface continuity at the TPCL. As discussed, $\mathscr{F}_{tot}$ alone cannot provide the equilibrium of the system, given the significance of non-variational terms associated with the active drops.

2.2. *Non-variational contributions and equilibrium*

For the active drop, the active stress ($\boldsymbol{\sigma}^a$) and the propulsion-related terms cannot be represented by variational calculations. Here, $\boldsymbol{\sigma}^a$ is experienced by the liquid drop due to the presence of the active particles inside the drop, ensuring that $\boldsymbol{p}$ and $\boldsymbol{\sigma}^a$ are related (see later) (Ravnik & Žumer 2009). Accordingly, using the work of Trinschek *et al.* (2020), we express the time variations of H and $\boldsymbol{p}$ in terms of the appropriate free energy gradients as

$$\partial_t H = \sum_k \partial_{x_k} \left[Q_{HH} \left(\partial_{x_k} \frac{\delta f}{\delta H} - \sum_j \partial_{x_k} \sigma^a_{kj} \right) + \sum_j Q_{HP_j} \partial_{x_k} \frac{\delta f}{\delta P_j} \right], \tag{2.12}$$

$$\partial_t P_i = \sum_k \partial_{x_k} \left[Q_{P_i H} \left(\partial_{x_k} \frac{\delta f}{\delta H} - \sum_j \partial_{x_k} \sigma^a_{kj} \right) + \sum_j Q_{P_i P_j} \partial_{x_k} \frac{\delta f}{\delta P_j} \right] - Q_{NC} \frac{\delta f}{\delta P_j}. \tag{2.13}$$

In (2.12) and (2.13), $\boldsymbol{P} = (H - h)\boldsymbol{p}$ is the height-averaged polarisation field, $\boldsymbol{\sigma}^a = -c_a \boldsymbol{pp}$, and $Q_{\alpha\beta}$ are the mobility coefficients (Trinschek *et al.* 2020). Here, $Q_{\alpha\beta}$ refers to the contribution of the variation of the free-energy with respect to the quantity β towards the time evolution of the quantity α. Also, Q_{NC} is the non-conservative term that accounts for the fact that $\boldsymbol{P}$ is not conserved over time. Considering a 2-D drop, where only the x-component of $\boldsymbol{P}$ is important (and hence we write $\boldsymbol{P} = P$), and solving for steady state ($\partial_t H = \partial_t P = 0$), we see that in general (i.e. when $Q_{HH}Q_{PP} \neq Q_{PH}Q_{HP}$ and $Q_{NC} \neq 0$), the only way the system can be in equilibrium is when

$$-\frac{Q_{HH}}{Q_{HP}} \left(\frac{\delta f}{\delta H} - \sigma^a_{xx} \right) = -\frac{\delta f}{\delta P} = A\mathrm{e}^{x\sqrt{c}} + B\mathrm{e}^{-x\sqrt{c}}, \tag{2.14}$$

where $c = Q_{NC}Q_{HH}/(Q_{PP}Q_{HH} - Q_{HP}Q_{PH})$, and A and B are arbitrary constants.

2.3. *Minimisation*

To obtain equilibrium, we take variations of f (or $\mathscr{F}_{tot}$) with respect to (w.r.t.) P, R, H and h. Normatively, free-energy is at a minimum at equilibrium. However, the active-stress (which is a result of active energy consumption by the active particles) pulls the system out of the minima and, therefore, instead of variation (of the free energy) w.r.t. H and P being zero, we get the equilibrium condition as (2.14). However, the free energy variation w.r.t. h and R still remain zero as there is no active energy consumption, i.e. no non-variational terms in the equilibrium condition for the elastic substrate or the drop edge. Considering the variation w.r.t P (remember, $\boldsymbol{P} = (H - h)\boldsymbol{p}$) yields (using (2.1) and (2.14))

$$-c_{sp2}p + c_{sp4}p^3 - c_p \frac{\left((H-h)p'\right)'}{H-h} = A\mathrm{e}^{x\sqrt{c}} + B\mathrm{e}^{-x\sqrt{c}}. \tag{2.15}$$

Considering the variation w.r.t. R yields

$$\left[\gamma_{SL}\sqrt{1+h'^2} + \gamma\sqrt{1+H'^2} + (\lambda_{SL} + \lambda_{SV})\,H'^2 - \lambda_{SL}h'^2\right]_{x=R^-} = \left[\gamma_{SV}\sqrt{1+h'^2} + \lambda_{SV}h'\right]_{x=R^+}. \tag{2.16}$$

Next, the variation w.r.t. H gives

$$\frac{\delta f}{\delta H} = -\frac{\gamma H''}{\left(1+H'^2\right)^{3/2}} - \mathbb{P} + c_{sp2}p^2 - c_{sp4}p^4, \tag{2.17}$$

$$\delta\mathcal{F}_{tot} = \left[\lambda_{SL} + \lambda_{SV} \pm \gamma \frac{H'(\pm R)}{\left(1+H'^2(\pm R)\right)^{1/2}}\right]\delta H(\pm R) + \int_{-R}^{R} \mathrm{d}x \frac{\delta f}{\delta H}\delta H(x). \tag{2.18}$$

As alluded, due to the non-variational terms, our variation in total energy w.r.t. $H(x)$ will be non-zero; hence, the variations are not equated to zero. However, at the TPCL, we have a localised surface tension force alone and no effect of polarisation field as per our energy functionals. For any variation in height near edges, $\delta H(\pm)$, $\mathscr{F}_{tot}$ must be constant as a small imaginary volume element at the drop edge experiencing only surface tension force must be in a net force balance. Hence, boundary terms in (2.18) reduce to

$$\lambda_{SL} + \lambda_{SV} = \gamma \frac{H'(-R)}{\sqrt{1+H'^2(-R)}} = \gamma \sin\theta. \tag{2.19}$$

Here, substituting (2.17) in (2.14), with negligible activity (c_{sp2}, c_{sp4}, $c_a \to 0$), we must have the excess pressure inside a drop satisfy $\mathbb{P} = \gamma \sin\theta/R = -\gamma H''/(1+H'^2)^{3/2}$, and since A,B are not functions of H or p, we conclude $A = B = 0$. Here, $\sin\theta/R$ is the drop curvature and $\mathbb{P} = \gamma \sin\theta/R$ represents the stress balance inside the drop (Joanny & Ramaswamy 2012; Chandel, Sivasankar & Das 2024).

Now, from (2.15) at steady state, we get $p = 0$ (isotropic state) and $p = \sqrt{c_{sp2}/c_{sp4}}$ (ordered state), which are the local maximum and the local minimum of $\mathscr{F}_{spo}$, respectively. Therefore, we use $p = \sqrt{c_{sp2}/c_{sp4}}$. Hence, from (2.17) and (2.14),

$$\frac{\gamma \sin\theta}{R}\left(1 + \frac{\Lambda}{\sin\theta}\right) = \mathbb{P} + \frac{c_{cp2}^2}{4c_{cp4}}, \tag{2.20}$$

where $\Lambda = Rc_a c_{cp2}/(4\gamma c_{cp4})$ is the active capillary number representing the ratio of the active stress to the capillary pressure. Equation (2.20) is the central result of this paper, showing the effect of activity in capillary pressure inside an active drop on a soft substrate. In (2.20), the right-hand side is the effective excess pressure with which the drop isotropically presses upon the substrate.

Finally, we perform variation w.r.t h, yielding

$$\begin{aligned}\delta\mathscr{F}_{tot} \;=\; & \left[\frac{\gamma_{SL}h'(R^-)}{\left(1+h'^2(R^-)\right)^{1/2}} - \lambda_{SL}\right]\delta h(R^-) - \left[\frac{\gamma_{SV}h'(R^+)}{\left(1+h'^2(R^+)\right)^{1/2}} - \lambda_{SV}\right]\delta h(R^+) \\ & - \int_{-\infty}^{\infty} dx \left[\frac{\gamma_s(x)h''(x)}{\left(1+h'^2(x)\right)^{3/2}} - \left(\mathbb{P} + \frac{c_{sp2}^2}{4c_{sp4}}\right)\Pi\left(\frac{x}{2R}\right)\right]\delta h(x) \\ & + \frac{1}{2}\int_{-\infty}^{\infty} \frac{\mathrm{d}q}{\sqrt{2\pi}\hat{K}(q)}\left[\delta\hat{h}(q)\hat{h}(-q) + \hat{h}(q)\delta\hat{h}(-q)\right] = 0.\end{aligned} \tag{2.21}$$

Equating the boundary terms in (2.21) to zero, along with $h'_{x=R^-} = \tan\theta_{SL}$ and $h'_{x=R^+} = \tan\theta_{SV}$, we obtain the Lagrange multipliers as $\lambda_{SL} = \gamma_{SL}\sin\theta_{SL}$ and $\lambda_{SV} = \gamma_{SV}\sin\theta_{SV}$, using which, we get the x-component of Young's equation, i.e.

$$\gamma_{SL}\cos\theta_{SL} + \gamma\cos\theta = \gamma_{SV}\cos\theta_{SV}. \tag{2.22}$$

Next, by substituting the expression for the Lagrange multipliers ($\lambda_{SL} = \gamma_{SL} \sin\theta_{SL}$ and $\lambda_{SV} = \gamma_{SV} \sin\theta_{SV}$) in (2.19), one can obtain

$$\gamma_{SL} \sin\theta_{SL} + \gamma_{SV} \sin\theta_{SV} = \gamma \sin\theta. \tag{2.23}$$

Equation (2.23) is the vertical component or the y-component of Young's equation. Thus, we find that the vertical component of the Young's equation is derived in a straightforward manner from the theory. However, note that this equation is not used in the following numerical calculations. Instead, for the numerical solutions, the necessary system of equations is completely defined just by the horizontal component of Young's equation (see (2.22)).

Following Jing *et al.* (2017), we express the integrand in (2.21) in terms of the wavenumber q using Fourier transform (with the symmetric convention) and further using (2.20), we get

$$\begin{aligned}
&\frac{1}{2}\int_{-\infty}^{\infty} \frac{\mathrm{d}q}{\sqrt{2\pi}\,\hat{K}(q)}\left[\delta\hat{h}(q)\hat{h}(-q) + \hat{h}(q)\delta\hat{h}(-q)\right] \\
&+ \int_{-\infty}^{\infty} \frac{\mathrm{d}q}{\sqrt{2\pi}}\left[q\left\{\hat{\gamma}_s(q) * \left(q\hat{h}(q)\right)\right\}\delta\hat{h}(q)\right] \\
&- \int_{-\infty}^{\infty} \mathrm{d}q\ \gamma\ \sin\theta\sqrt{\frac{2}{\pi}}\left[\exp\left(-\frac{1}{2a^2q^2}\right)\cos Rq - \left(1 + \frac{\Lambda}{\sin\theta}\right)\mathrm{sinc}\ Rq\right]\delta\hat{h}(q) = 0.
\end{aligned} \tag{2.24}$$

Here, a is an infinitesimal width of the Gaussian used to approximate the concentrated force at the TPCL. Since we consider nematic particles, we expect the drop to be symmetric around the centre. Given that our entire starting system, namely the drop, substrate and the arrangement of active particles, is symmetric about origin, we can safely expect our solution for the drop shape to be symmetric as well. Therefore, $h(x)$ will be real and even, implying $h((q)$ to be real and even. This leaves the integrand in (2.24) as

$$\begin{aligned}
&\frac{\hat{h}(q)}{\sqrt{2\pi}\,\hat{K}(q)} + \frac{q\hat{\gamma}_s(q) * \left(q\hat{h}(q)\right)}{\sqrt{2\pi}} \\
&\quad - \frac{\gamma\ \sin\theta}{\sqrt{\pi/2}}\left[\exp\left(\frac{-1}{2a^2q^2}\right)\cos Rq - \left(1 + \frac{\Lambda}{\sin\theta}\right)\mathrm{sinc}\ Rq\right] = 0.
\end{aligned} \tag{2.25}$$

Accordingly, after isolating the $\hat{h}(q)$ from (2.25), the final equilibrium equation reads as

$$\hat{h}(q) = \left[\frac{\sqrt{2\pi}\,\hat{K}(q)\,\hat{f}_n(q,a)}{1 + \gamma_{SV}q^2\hat{K}(q)}\right], \tag{2.26}$$

$$\begin{aligned}
\hat{f}_n(q,a) = {}& \gamma\ \sin\theta\sqrt{\frac{2}{\pi}}\left[\exp\left(-\frac{1}{2a^2q^2}\right)\cos Rq - \left(1 + \frac{\Lambda}{\sin\theta}\right)\mathrm{sinc}\ Rq\right] \\
&- (\gamma_{SV} - \gamma_{SL})\sqrt{\frac{2}{\pi}}\frac{\left[q\left[\mathrm{sinc}(q) * \left(q\hat{h}(q)\right)\right]\right]}{\sqrt{2\pi}}.
\end{aligned} \tag{2.27}$$

This gives us all the necessary equations needed to solve (iteratively) for the drop and the solid shapes. We first guess a value for θ, solve for $\hat{h}(q)$ (using (2.26)) over a range of wave numbers (we used $q = \{-16 \times 10^4$ to $16 \times 10^4\}$ in increments of 0.25). We then

obtain $h(x)$ from $\hat{h}(q)$. With $h(x)$ known, we know $\tan\theta_{SL}$ and $\tan\theta_{SV}$, and, hence, θ from (2.22). We now use this θ to get a better approximation for $\hat{h}(q)$, which will give us a better approximation for θ. We see that one gets a stable solution for the shape of our system regardless of initial guess value of θ. The radius corresponding to $\Lambda = 0$ is noted as R_0. For non-zero values of Λ, we repeat the above-mentioned process by varying the radius by $R_0 \to R(\Lambda)$ iteratively, till the volume is matched to an accuracy of 10^{-6} of relative error in volume. For a detailed derivation of Fourier transformation of the free energies, we request the readers to read our previous paper (Jing *et al.* 2017).

3. Results

We study the behaviour of the active-drop–soft-substrate system by making our system dimensionless (variables with tilde overhead) as $(\tilde{h}, \tilde{H}, \tilde{x}, \tilde{R}) = (h, H, x, R)/R_0$. The system, as expected, gives a steady-state solution in its ordered state. This state corresponds to low noise/turbulence in the active system (or the low-temperature state if drawn an analogy with liquid-crystal theory). In the ordered state, we get a simple analytical solution to the polarisation field, enabling us to analyse various properties of the active-drop–soft-substrate system. We first demonstrate the shape of the drop on the soft substrate for the extensile drop ($\Lambda > 0$) (figure 2*d*) and the contractile drop ($\Lambda < 0$) (figure 2*a*,*b*) in contrast to the neutral drop ($\Lambda = 0$) (figure 2*c*) for elasto-capillary number ($\gamma/(ER_0)$) of 0.1. As compared to the neutral drops, the drop flattens out corresponding to extensile activity. However, for the case of the contractile activity, as compared to neutral drops, the drop thickens (for smaller $|\Lambda|$) or the substrate gets lifted (for larger $|\Lambda|$).

We next compare similar drops of a given volume corresponding to varying activities for different values of $\gamma/(ER_0)$ (see figure 2*e*). As compared to the neutral drops, the dimensionless radius $\tilde{R}$ increases for the active drops with extensile activity, as for this case, the active drop presses deeper into soft surface (compare figure 2*c* and 2*d*). However, for the drop with contractile, i.e. negative activity, as compared to the neutral case, the dimensionless radius $\tilde{R}$ decreases for smaller $|\Lambda|$ (for this case, the drop bulges out more from the soft surface) (compare figures 2*b* and 2*c*) and increases for larger $|\Lambda|$ (for this case, the soft surface itself gets lifted up) (compare figures 2*a* and 2*c*). The greater the value of $\gamma/(ER_0)$, the more prominent is this effect. Also, this result suggests that as compared to a neutral drop, the active drop with extensile activity wets the soft surface more, while the active drop with contractile activity de-wets (wets) the soft surface more for smaller (larger) $|\Lambda|$.

Such enhanced wetting/dewetting can be mechanistically understood by observing the contact angles at the TPCL. In regular drops, the excess pressure inside the drop is directly proportional to the contact angle θ for a given radius R. However, from (2.20), we see that for a fixed radius and a fixed contact angle, the excess pressure (term appearing on the right-hand side of (2.20)) inside the drop increases linearly with the active stress (Λ) for extensile drops ($\Lambda > 0$). Let us increase the activity Λ from zero to a positive value and see what happens. This will pushes the substrate down and consequently increase the solid–liquid contact angle θ_{SL} (see figure 2*g*). However, now we must realise that the contact angle and the radius will change if the substrate is pushed down as a result of the increased activity. Under such circumstances, according to the x-component of Young's equation (see (2.22)), there will be a decrease in θ and θ_{SV} by a similar amount (see figure 2*g*,*h*). This increase in θ_{SL} for a fixed R results in an increased volume of the drop, while the decrease in θ would result in a decrease in the drop volume. Evidently, from the numerics, the gain in the drop volume due to an increase in θ_{SL} is less than the loss in drop volume

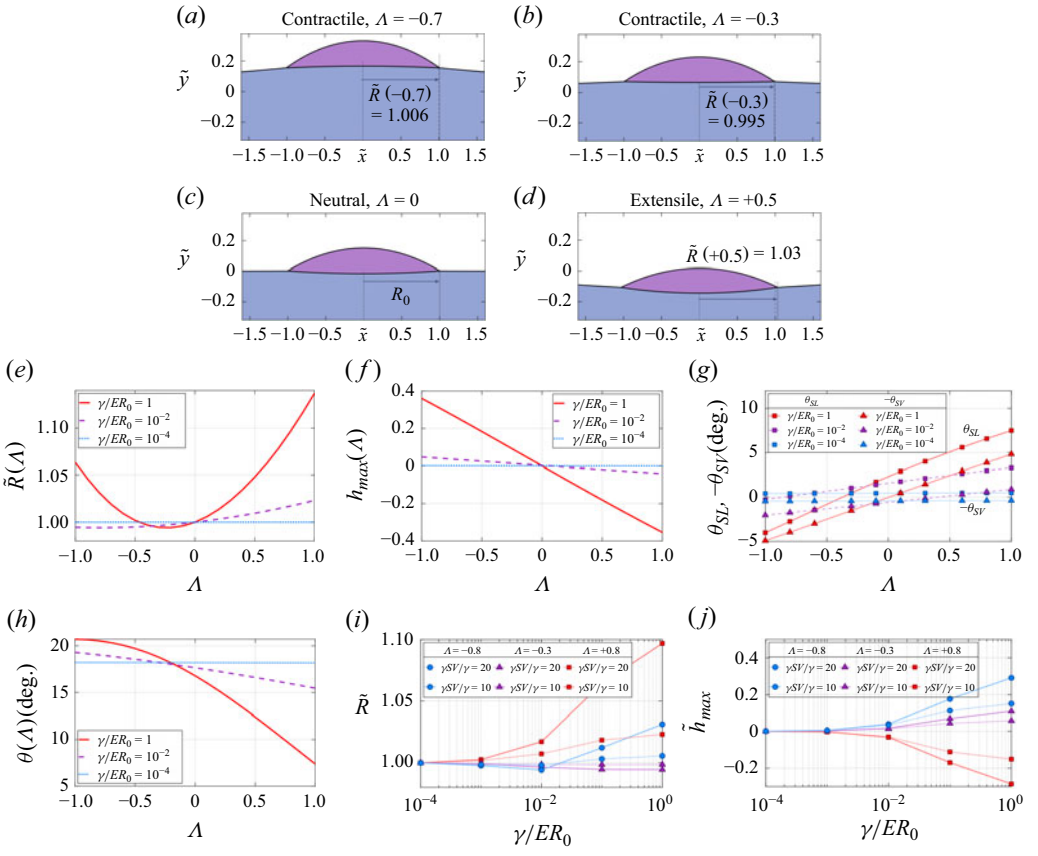

Figure 2. (*a–d*) Equilibrium shapes for (*a*) contractile ($\Lambda = -0.7 < 0$), (*b*) contractile ($\Lambda = -0.3$), (*c*) neutral ($\Lambda = 0$), and (*d*) extensile ($\Lambda = 0.5 > 0$) drops for $\gamma/(ER_0) = 0.1$ and $\gamma_{SV}/\gamma = 10$. (*e*) Variation of the dimensionless wetting radius ($\tilde{R} = R/R_0$) with Λ for different values of $\gamma/(ER_0)$. (*f*) Variation of the dimensionless height of TPCL ($\tilde{h}_{max} = h(R)/R_0$) with Λ for different $\gamma/(ER_0)$. (*g*) Variation of the solid–liquid (θ_{SL}) and solid–vapour (θ_{SV}) contact angles with Λ for different $\gamma/(ER_0)$. (*h*) Variation of the contact angle (θ) with Λ for different $\gamma/(ER_0)$. In panels (*a*)–(*h*), $\gamma_{SV}/\gamma = 10$. (*i*) Variation of $\tilde{R}$ with $\gamma/(ER_0)$ for various γ_{SV}/γ. (*j*) Variation of $\tilde{h}_{max}$ with $\gamma/(ER_0)$ for various γ_{SV}/γ. In panels (*i*) and (*j*), the cases of contractile and extensile activities have been identified by their corresponding markers as shown in the legend. In all the cases shown from panels (*a*)–(*j*), we have kept the ratio, $(\gamma_{SV} - \gamma_{SL})/\gamma = 0.95$, i.e. constant.

due to a decrease in θ, resulting in a smaller overall drop volume for a fixed drop radius. Therefore, with increased excess pressure due to active stress for an extensile drop, the drop expands in radius R to accommodate for the lost volume. This explains the variation in R with Λ for extensile drops (see figure 2*e*). This also accounts for the drop shape illustrated in figure 2(*d*).

We next consider the case of contractile drops ($\Lambda < 0$) for relatively small values of $|\Lambda|$, i.e. $|\Lambda|$ is small enough so that $\gamma \sin\theta/R + \Lambda\gamma/R$ (or the left-hand side of (2.20)) remains positive. Under such circumstances, the pressure (appearing on the right-hand side of (2.20)) inside the drop decreases linearly with decreasing the active stress (Λ) ($\Lambda < 0$). This makes the drop bulge out of the soft surface and decreases the solid–liquid contact angle θ_{SL} and increases θ and θ_{SV} (using the x-component of Young's equation or (2.22)). The decrease in θ_{SL} for a fixed R decreases the drop volume, while the increase in θ increases the drop volume. Numerically, in the region of ($\Lambda < 0$), where the excess

pressure is still positive, the effect of the increase in θ dominates; accordingly, the drop increases in volume. Therefore, with a decreased excess pressure (for the contractile drops with smaller $|\Lambda|$), the drop contracts in radius R (and bulges out from the soft surface) to compensate for the gained volume. This explains the variation in R with Λ for contractile drops with small $|\Lambda|$ (see figure 2*e*). This also explains the drop shape illustrated in figure 2(*b*).

This numerical trend described here holds for the increase/decrease in the drop radius in the region where $1 + \Lambda/\sin\theta > 0$ (or $\gamma \sin\theta/R + \Lambda\gamma/R > 0$), which may not always be the case. For example, for contractile drops with sufficiently large magnitude of $|\Lambda|$ or sufficiently small θ (i.e. sufficiently flat drop), we may have $\gamma \sin\theta/R + \Lambda\gamma/R < 0$. As we see from figure 2(*e*), for such drops with sufficiently negative (contractile) activity Λ, the radius increases with an increase in the negative magnitude of the activity. This is because, for sufficiently negative Λ, the excess pressure inside the drop becomes negative and thus, not only the drop, but the substrate as well bulges upwards. Numerically, we find that a further decrease in Λ increases both θ and θ_{SL} (i.e. increases the negative magnitude of θ_{SL}) with an overall decrease in the volume, which is compensated by an increase in $\tilde{R}$ to ensure the conservation of the drop volume. The physical representation of this drop–substrate deformation is shown in figure 2(*a*).

Thus, as compared to a neutral drop, an extensile drop pushes the substrate with a greater overall downward force, thereby justifying the drop pressing deeper into the soft substrate (figure 2*c*,*d*); as a result, for extensile drops, the dimensionless height of TPCL ($\tilde{h}_{max} = h(R)/R_0$) becomes progressively more negative with an increase in Λ (see figure 2*f*). However, depending on the negative magnitude of Λ, the contractile drop either pushes the substrate with much lesser pressure (as compared to the neutral drop) and comes out of the soft surface (this scenario occurs for smaller $|\Lambda|$; see figure 2*b*,*c*), or makes the soft surface itself bulge out (this scenario occurs for larger $|\Lambda|$; see figure 2*a*,*c*). Both these effects associated with the contractile drop increase the height the dimensionless height of the TPCL ($\tilde{h}_{max}$), with the larger increase occurring for the case where the substrate bulges out. As a result, we obtain a progressive increase in $\tilde{h}_{max}$ for progressively more negative values of Λ (figure 2*f*).

Next, for the contact angles, we have already discussed how the x-component of Young's law governs the relative variation of θ_{SL}, θ_{SV} and θ (please see the above-mentioned discussions for figure 2*e*). Given the fact that this balance holds regardless of the softness of the substrate, or the magnitude or sign of the activity, implies that a variation of these components (namely, the substrate softness and the value of Λ) causes a rotation of the contact line at the drop corner. We plot these angles (θ_{SL}, θ_{SV} and θ) in figure 2(*g*,*h*). The dependence of θ_{SL} and θ_{SV} on the nature of the activity has already been discussed previously (please see the above-mentioned discussions for figure 2*e*). With regards to the variation in θ, intuitively, the contractile drop increases the contact angle (as it either pops out of the soft surface for small $|\Lambda|$ or bulges the substrate itself for large $|\Lambda|$), while the extensile drop decreases the angle (as it goes deeper into the soft substrate; figure 2*h*).

Please note that while the streamwise component of the Young's equation (see (2.22)) is used to obtain the numerical results for the different contact angles, these results also approximately satisfy the cross-stream component of Young's equation (see (2.23)) for the parameter combinations considered in this paper. For example, using (2.22) and (2.23), we can eliminate θ and can write the following equation:

$$\cos(\theta_{SL} + \theta_{SV}) = \frac{\gamma_{SL}^2 + \gamma_{SV}^2 - \gamma^2}{2\gamma_{SL}\gamma_{SV}} = \text{constant}. \tag{3.1}$$

In figure 2(*g*), we find that the maximum and minimum values of $|\theta_{SL}+\theta_{SV}|$ are 3° and 0°, respectively, making the maximum and minimum values of (numerically obtained) cos $(\theta_{SL}+\theta_{SV})$ as 1 and 0.9986, respectively. Hence, (the numerically obtained) cos $(\theta_{SL}+\theta_{SV})$ is effectively constant and, hence, satisfies (2.23) in the range of $|\Lambda|$ and $\gamma/(ER_0)$ values considered here. Of course, the values of cos $(\theta_{SL}+\theta_{SV})$ will become more deviated from 1 for softer surfaces (i.e. smaller values of $\gamma/(ER_0)$) and for greater activity values (or $|\Lambda|>1$); hence, for such values of $\gamma/(ER_0)$ and Λ, the numerical results might not stringently satisfy (2.23). In this context, it is also useful to point out that for thicker drops on extremely rigid surfaces (or $\gamma/(ER_0)\to 0$), (2.23) yields $\theta=0$ since for such cases, there is no solid deformation and $\theta_{SL}=\theta_{SV}=0$. However, for such surfaces, $\theta=\theta_Y=\cos^{-1}((\gamma_{SV}-\gamma_{SL})/\gamma)$, where θ_Y is Young's angle. Therefore, it must be noted that the theory cannot be trivially extended to very rigid surfaces for thicker drops.

Finally, we plot the behaviour of an active drop (i.e. quantify $\tilde{R}$ and $\tilde{h}_{max}$) as a function stiffness of the substrate in figure 2(*i*,*j*). We consider the three distinct situations encountered in the present problem: case of extensile drop ($\Lambda>0$) (drop profile shown in figure 2*d*), case of contractile drop with a smaller magnitude of Λ ($\Lambda=-0.3$) (drop profile shown in figure 2*b*) and case of contractile drop with a larger magnitude of Λ ($\Lambda=-0.7$) (drop profile shown in figure 2*a*). We see that for all the cases, the system asymptotically attains fixed values of $\tilde{R}$ and $\tilde{h}_{max}$ in the limit of extremely stiff substrate ($\gamma/ER_0\to 0$), which in a loose sense represents an error-function (this is what one must expect as an extremely stiff substrate is equivalent to a rigid solid). Also, as has been already shown in figure 2(*e*,*f*), a softer surface (or a larger value of γ/ER_0) enhances the corresponding variation of $\tilde{R}$ and $\tilde{h}_{max}$ at a given Λ value. Hence, for the extensile drop ($\Lambda=0.8$), $\tilde{R}$ progressively increases and $\tilde{h}_{max}$ progressively decreases (i.e. becomes increasingly more negative) with an increase in the softness. Similarly, with an increase in the softness, for the contractile drops, for a smaller magnitude of $|\Lambda|$ (or $\Lambda=-0.3$), $\tilde{R}$ decreases progressively (i.e. becomes less than unity) and $\tilde{h}_{max}$ (weakly) increases progressively. For the same contractile drops, but with a greater magnitude of $|\Lambda|$ (or $\Lambda=-0.8$) (i.e. conditions for which the substrate itself bulges), an increase in the softness (corresponding to $\gamma/ER_0>0.01$) progressively increases $\tilde{R}$ and $\tilde{h}_{max}$. Overall, we see that for drops bounded by surface tension, the active stresses do not stretch or squish the underlying solid directly; rather, the active stresses decrease (increase) the pressure employed by the drop on the substrate for a contractile (extensile) drop and the result is the drop coming out of the solid or bulging the solid itself (for contractile drops) and the drop pressing deeper into the solid (for extensile drops). This understanding extends even to non-uniform polarisation field, where we can expect active stresses to locally compensate (or counterpose) for the nearby curvatures by the same mechanism as described by (2.20).

4. Conclusion

The seemingly omnipresence of active matter in biological and chemical systems necessitates the treatment of active matter in conjunction to soft substrates. Here, we provide the first mathematical framework for capturing the interaction of an active drop (matter) with soft substrates. We find the validity of Young's equation in its unaltered form for 2-D drops and the mechanism of drop spreading and impinging on surfaces through equations that can be solved semi-analytically, thereby illuminatingly revealing the system. Such a study shows the importance of elasticity in determining the dynamics of colonies of active cells, provides a first-principles foundation for understanding the

growth of embryos over uterus (Guruciaga *et al.* 2024), and has potential impact on periodic motion (Memarian *et al.* 2024), chaotic mixing (Mitchell *et al.* 2024) and other facets of the growing field of active nematics. In future studies, it would be remarkable to obtain non-equilibrium solutions to the active arrangement and possibly extend the solution to three dimensions, which would be a first-principles solution to the formation of multi-cellular organisms.

Supplementary material. Supplementary material is available at https://doi.org/10.1017/jfm.2025.10624.

Declaration of Interests. The authors report no conflict of interest.

References

Balasubramaniam, L., Mège, R.-M. & Ladoux, B. 2022 Active nematics across scales from cytoskeleton organization to tissue morphogenesis. *Curr. Opin. Genet. Develop.* **73**, 101897.

Bazellières, E. *et al.* 2015 Control of cell–cell forces and collective cell dynamics by the intercellular adhesome. *Nat. Cell Biol.* **17** (4), 409–420.

Chandel, G.R., Sivasankar, V.S. & Das, S. 2024 Evaporation of active drops: puncturing drops and particle deposits of ring galaxy patterns. *Phys. Rev. Fluids* **9** (3), 033603.

Drescher, K., Dunkel, J., Cisneros, L.H., Ganguly, S. & Goldstein, R.E. 2011 Fluid dynamics and noise in bacterial cell–cell and cell–surface scattering. *Proc. Natl Acad. Sci.* **108** (27), 10940–10945.

Guillamat, P., Blanch-Mercader, C., Pernollet, G., Kruse, K. & Roux, A. 2022 Integer topological defects organize stresses driving tissue morphogenesis. *Nat. Mater.* **21** (5), 588–597.

Guruciaga, P.C., Ichikawa, T., Hiiragi, T. & Erzberger, A. 2024 Boundary geometry controls topological defect transitions that determine lumen nucleation in embryonic development. arXiv: 2403.08710

Ichikawa, T. *et al.* 2022 An exA0;vivo system to study cellular dynamics underlying mouse peri-implantation development. *Develop. Cell* **57** (3), 373–386.

Jerison, E.R., Xu, Y., Wilen, L.A. & Dufresne, E.R. 2011 Deformation of an elastic substrate by a three-phase contact line. *Phys. Rev. Lett.* **106** (18), 186103.

Jing, H., Sinha, S. & Das, S. 2017 Elasto-electro-capillarity: drop equilibrium on a charged, elastic solid. *Soft Matter* **13** (3), 554–566.

Joanny, J.-F. & Ramaswamy, S. 2012 A drop of active matter. *J. Fluid Mech.* **705**, 46–57.

Kim, K., Yoshinaga, N., Bhattacharyya, S., Nakazawa, H., Umetsu, M. & Teizer, W. 2018 Large-scale chirality in an active layer of microtubules and kinesin motor proteins. *Soft Matter* **14** (17), 3221–3231.

Latorre, E. *et al.* 2018 Active superelasticity in three-dimensional epithelia of controlled shape. *Nature* **563** (7730), 203–208.

Levental, I., Georges, P.C. & Janmey, P.A. 2007 Soft biological materials and their impact on cell function. *Soft Matter* **3** (3), 299–306.

Lubbers, L.A., Weijs, J.H., Botto, L., Das, S., Andreotti, B. & Snoeijer, J.H. 2014 Drops on soft solids: free energy and double transition of contact angles. *J. Fluid Mech.* **747**, R1.

Memarian, F.L., Hammar, D., Sabbir, M.M.H., Elias, M., Mitchell, K.A. & Hirst, L.S. 2024 Controlling chaos: periodic defect braiding in active nematics confined to a cardioid. *Phys. Rev. Lett.* **132** (22), 228301.

Mitchell, K.A., Sabbir, M.M.H., Geumhan, K., Smith, S.A., Klein, B. & Beller, D.A. 2024 Maximally mixing active nematics. *Phys. Rev. E* **109** (1), 014606.

Peng, C., Turiv, T., Guo, Y., Wei, Q.-H. & Lavrentovich, O.D. 2016 Command of active matter by topological defects and patterns. *Science* **354** (6314), 882–885.

Pérez-González, C., Alert, R., Blanch-Mercader, C., Gómez-González, M., Kolodziej, T., Bazellieres, E., Casademunt, J. & Trepat, X. 2019 Active wetting of epithelial tissues. *Nat. Phys.* **15** (1), 79–88.

Ramaswamy, S. 2010 The mechanics and statistics of active matter. *Annu. Rev. Condens. Matter Phys.* **1** (1), 323–345.

Ravnik, M. & Žumer, S. 2009 Landau–de Gennes modelling of nematic liquid crystal colloids. *Liq. Cryst.* **36** (10-11), 1201–1214.

Saw, T.B., Doostmohammadi, A., Nier, V., Kocgozlu, L., Thampi, S., Toyama, Y., Marcq, P., Lim, C.T., Yeomans, J.M. & Ladoux, B. 2017 Topological defects in epithelia govern cell death and extrusion. *Nature* **544** (7649), 212–216.

Sengupta, A. 2020 Microbial active matter: a topological framework. *Frontiers Phys.* **8**, 184.

SINGH, G. & CHANDA, A. 2021 Mechanical properties of whole-body soft human tissues: a review. *Biomed. Mater.* **16** (6), 062004.

SOOFI, S.S., LAST, J.A., LILIENSIEK, S.J., NEALEY, P.F. & MURPHY, C.J. 2009 The elastic modulus of Matrigel^{TM} as determined by atomic force microscopy. *J. Struct. Biol.* **167** (3), 216–219.

TAN, A.J., ROBERTS, E., SMITH, S.A., OLVERA, U.A., ARTEAGA, J., FORTINI, S., MITCHELL, K.A. & HIRST, L.S. 2019 Topological chaos in active nematics. *Nat. Phys.* **15** (10), 1033–1039.

TREPAT, X., WASSERMAN, M.R., ANGELINI, T.E., MILLET, E., WEITZ, D.A., BUTLER, J.P. & FREDBERG, J.J. 2009 Physical forces during collective cell migration. *Nat. Phys.* **5** (6), 426–430.

TRINSCHEK, S., STEGEMERTEN, F., JOHN, K. & THIELE, U. 2020 Thin-film modeling of resting and moving active droplets. *Phys. Rev. E* **101** (6), 062802.